Biomaterials 235 (2020) 119794

Contents lists available at ScienceDirect

Biomaterials

journal homepage: www.elsevier.com/locate/biomaterials

Injectable hydrogel enables local and sustained co-delivery to the brain: Two clinically approved biomolecules, cyclosporine and erythropoietin, accelerate functional recovery in rat model of stroke

Anup Tuladhar[a,f], Jaclyn M. Obermeyer[a,b,f], Samantha L. Payne[a,b,f], Ricky C.W. Siu[b], Sohrab Zand[c], Cindi M. Morshead[a,e,f], Molly S. Shoichet[a,b,d,e,*]

[a] Institute of Biomaterials and Biomedical Engineering, University of Toronto, 164 College Street, Toronto, ON, M5S 3G9, Canada
[b] Department of Chemical Engineering and Applied Chemistry, University of Toronto, 200 College Street, Toronto, ON, M5S 3E5, Canada
[c] Department of Human Biology, University of Toronto, 300 Huron Street, Toronto, ON, M5S 3E5, Canada
[d] Department of Chemistry, University of Toronto, 80 St. George Street, Toronto, ON, M5S 3H6, Canada
[e] Department of Surgery, University of Toronto, 149 College Street, Toronto, ON, M5S 3E1, Canada
[f] Donnelly Centre for Cellular and Biomolecular Research, University of Toronto, 160 College Street, Toronto, ON, M5S 3E1, Canada

ARTICLE INFO

Keywords:
Hyaluronan
Methyl cellulose
Drug delivery
Cyclosporine
Erythropoietin
Stroke recovery

ABSTRACT

Therapeutic delivery to the brain is limited by the blood-brain barrier and is exacerbated by off-target effects associated with systemic delivery, thereby precluding many potential therapies from even being tested. Given the systemic side effects of cyclosporine and erythropoietin, systemic administration would be precluded in the context of stroke, leaving only the possibility of local delivery. We wondered if direct delivery to the brain would allow new reparative therapeutics, such as these, to be identified for stroke. Using a rodent model of stroke, we employed an injectable drug delivery hydrogel strategy to circumvent the blood-brain barrier and thereby achieved, for the first time, local and sustained co-release to the brain of cyclosporine and erythropoietin. Both drugs diffused to the sub-cortical neural stem and progenitor cell (NSPC) niche and were present in the brain for at least 32 days post-stroke. Each drug had a different outcome on brain tissue: cyclosporine increased plasticity in the striatum while erythropoietin stimulated endogenous NSPCs. Only their co-delivery, but not either drug alone, accelerated functional recovery and improved tissue repair. This platform opens avenues for hitherto untested therapeutic combinations to promote regeneration and repair after stroke.

1. Introduction

Drug development for stroke - the most prevalent cause of permanent disability [1] - has been severely impeded and is further complicated by the blood-brain barrier (BBB), which prevents most therapeutics from freely diffusing into the brain parenchyma. Thus, only biomolecules that are either able to penetrate the BBB or delivered in conjunction with methods that disrupt the BBB have been investigated. However, many compounds predicted to cross the BBB are removed by efflux transporters, such as p-glycoproteins and multidrug resistance associated proteins [2]. Generalized BBB disruption, such as with a hyperosmolar solution, increases drug accumulation in the brain [3], but regional variation in permeabilisation and the risks associated with generalized BBB opening make this approach unreliable [4]. Focused ultrasound has shown promise for localized and reversible BBB disruption, allowing well-controlled and spatially localized drug penetration into the brain [5]; yet, poor serum stability and the associated risks of systemic exposure for broadly acting therapeutics are still unaddressed by these improvements.

With local delivery, the drug bypasses the BBB and can rapidly accumulate in the brain parenchyma [6]. Ventricular infusion through a catheter and osmotic minipump system, such as the clinically-used Ommaya reservoir, has been used to achieve local delivery to the brain [7]; however, in these studies the drug concentration and distribution within the brain were not quantified. Since ventricular infusates are often rapidly cleared into the blood stream through the choroid plexus, drug accumulation in the brain parenchyma is limited, and delivery is more akin to that of sustained intravenous infusion than local delivery [8]. With the Ommaya reservoir, brain tissue is damaged and cerebral infection rates increased [9].

To address the challenges associated with drug delivery to the brain, we developed a minimally-invasive local delivery platform to

* Corresponding author. Department of Chemical Engineering and Applied Chemistry, University of Toronto, 200 College Street, Toronto, ON, M5S 3E5, Canada.
E-mail address: molly.shoichet@utoronto.ca (M.S. Shoichet).

https://doi.org/10.1016/j.biomaterials.2020.119794
Received 21 June 2019; Received in revised form 6 January 2020; Accepted 15 January 2020
Available online 16 January 2020
0142-9612/

circumvent the BBB, both minimizing systemic drug exposure and increasing drug concentration at the site of action [6,10–16]. The platform uses a biocompatible hydrogel drug depot, comprised of hyaluronan and methylcellulose (HAMC). Unlike intracranial hydrogel delivery approaches [17–25], the HAMC hydrogel is deposited onto the surface of the brain, avoiding the tissue damage that typically occurs from intracranial implants [14,26]. HAMC is a physically cross-linked, in situ gelling polymer blend that forms by inverse thermal gelation. Drug release from the gel can be fine-tuned on the order of days to months by controlling how drugs are formulated inside the gel, either in free form or encapsulated in polymeric particles [27]. Multi-drug release is achieved by mixing different biomolecules and/or drug-loaded particles within the gel [14,28,29].

In this study, we sought to determine if the platform could be used to develop new reparative therapies for stroke. Current stroke treatments target tissue sparing with pharmacological or surgical thrombolysis, but are only effective within the first few hours of injury [30] and do not aid in tissue regeneration. Endogenous repair processes in pre-clinical models of stroke can be stimulated by small molecules, proteins, or peptides [31] by targeting endogenous neural stem and progenitor cells (NSPCs), axonal sprouting, synaptogenesis, or removal of growth inhibitory cues. Cyclosporine (CsA) is a common immunosuppressant and has been shown to stimulate the endogenous stem cells in the rodent brain [32–34]. Erythropoietin (EPO) stimulates red blood cell production and has been shown to promote neurogenesis in the rodent brain [35–37]. Both drugs are neuroprotective after stroke when administered within the first 24 h after injury [33,34,36,38]. Single drug delivery of either CsA [33,34] or EPO [36] for 7–32 days systemically has been shown to promote neuroprotection and functional recovery after stroke. Additionally, combined CsA and EPO delivery, by systemic intra-peritoneal or subcutaneous injections for up to 48 h after stroke, demonstrated that combined CsA + EPO treatment had a greater neuroprotective effect than either drug alone [38].

We wondered whether the co-delivery of CsA and EPO, administered 4 days after injury and outside the neuroprotective window [39], would be efficacious for tissue repair and functional recovery after stroke given that they should target multiple repair pathways. However, systemic delivery of both CsA and EPO is untenable in humans because not only would there be low levels of the biomolecules in the brain, but CsA [40] would also cause immunosuppression in vulnerable stroke patients [41,42] while EPO would increase red blood cell density [43], which could lead to secondary ischemic occlusion and injury [44]. Thus, a local delivery strategy was necessary in order to even investigate the combined benefit of CsA and EPO co-delivery.

We synthesized a composite hydrogel for injection directly onto (but not into) the brain cortex, comprised of drug-loaded poly(lactide-co-glycolide) (PLGA) particles that were then dispersed in HAMC. As we were interested in studying the effects of single vs. dual drug treatment, and as co-encapsulation in PLGA could affect drug loading and release [45], we designed the system to be modular: CsA and EPO were independently encapsulated in separate PLGA particles. Single or dual drug release is achieved by mixing different drug-loaded PLGA particles in the HAMC hydrogel. The total amount of PLGA was kept constant (20% w/v) by adding a balance of blank PLGA particles, where necessary, to control for any impact of particle degradation on release and/or brain tissue [46]. While no animal model is perfect, we used an endothelin-1 model of focal ischemia because it produces injuries that are of similar relative size to treatable human stroke (4.5–14% of the affected hemisphere) and mimics the gradual reperfusion seen in human ischemic stroke [47,48].

Neuronal cell death in this endothelin-1 injury model occurs primarily within the first 24 h after stroke [48]. In order to investigate the regenerative (vs. protective) effects of locally delivered CsA and EPO, we began delivery at 4 days post-injury. We show that the platform can provide sustained local delivery to the brain for one month, at concentrations unachievable with systemic delivery, with the biomolecules reaching the subventricular zone of the lateral ventricles where the endogenous stem cells are found. Importantly, we demonstrate, for the first time, that the combination of two clinically used drugs, CsA and EPO, but not each drug alone, accelerates functional recovery and promotes tissue repair after stroke in an endothelin-1 rat model.

2. Methods

All reagents were purchased from Sigma-Aldrich (Oakville, ON, Canada), unless specified otherwise.

2.1. CsA encapsulation in PLGA microparticles

CsA (Cat.#C-6000, *LC Laboratories*, Woburn, MA, USA) was encapsulated in PLGA (acid-terminated 50:50, MW 7000–17,000, Cat.#71989) microparticles using a single-emulsion oil/water solvent evaporation method, as previously described [13]. Blank PLGA CsA-formulation particles were similarly prepared without the addition of CsA in the organic phase. Mean particle sizes were between 14.7 and 25.0 μm [6,13].

2.2. EPO encapsulation in PLGA microparticles

Sterile EPO solution (40,000 IU/mL, EPREX epoetin alfa, *Janssen Inc*, Toronto, ON, Canada) was ejected into a sterile 2 mL Max-Recovery tube and lyophilized within a sterile container. Dry EPO was reconstituted with 100 μL of sterile artificial cerebrospinal fluid (aCSF: 148 mM NaCl, 3 mM KCl, 0.8 mM $MgCl_2$, 1.4 mM $CaCl_2$, 1.5 mM Na_2HPO_4, 0.2 mM NaH_2PO_4 in ddH_2O, pH adjusted to 7.4, filter sterilized at 0.2 μm [26,49]) containing 0.1% BSA. EPO (40,000 IU) was encapsulated in PLGA microparticles (120 mg) using a double-emulsion water/oil/water solvent evaporation method, as previously described [14]. Blank PLGA EPO-formulation particles were similarly prepared without the addition of EPO in the aqueous phase. Mean particle sizes were 18 ± 4.7 μm [14].

2.3. Preparation of sterile HAMC

Sterile hyaluronan (HA, 1.4–1.8 × 10^6 g/mol, Pharmagrade 150 sodium hyaluronate, *NovaMatrix*, Sandvika, Norway), and methylcellulose (MC, 3.4 × 10^5 g/mol, Cat.#SM-4000-C, *Shin Etsu*, Chiyoda-ku, Tokyo, Japan) were formulated independently at 1.4 wt/vol% HA and 3.0 wt/vol% MC, as previously described [6].

2.4. Preparation of drug delivery gel

The HAMC gel used for CsA + EPO treated animals contained 10% w/v CsA-loaded PLGA microparticles (49.2 μg CsA per animal) and 10% w/v EPO-loaded PLGA microparticles (5.6 ng EPO per animal). The HAMC gel used for CsA-only treated animals contained 10% w/v CsA-loaded PLGA microparticles (49.2 μg CsA per animal) and 10% w/v blank PLGA "EPO-formulation" microparticles (0 ng EPO per animal). The HAMC gel used for EPO-only treated animals contained 10% w/v EPO-loaded PLGA microparticles (5.6 ng EPO per animal) and 10% w/v blank PLGA "CsA-formulation" microparticles (0 μg CsA per animal). Vehicle treated animals only had blank PLGA particles dispersed in HAMC, with 10% w/v blank PLGA "CsA-formulation" microparticles (0 μg CsA per animal) and 10% w/v blank PLGA "EPO-formulation" microparticles (0 ng EPO per animal). Thus, all gels contained 20% w/v PLGA particles.

2.5. Animal approval

All animal work was carried out in accordance with the Guide to the Care and Use of Experimental Animals (Canadian Council on Animal Care) and approved by the Animal Care Committee at the University of

Toronto. A total of 232 male Sprague Dawley rats and 10 male Long-Evans rats (Charles River, QC, Canada) were used in these studies. Guidelines for experimental stroke from the Stroke Therapy Academic Industry Roundtable (STAIR) were taken into consideration when designing animal experiments, including: randomization of animals into experimental groups, use of inclusion and exclusion criteria, justified choice of therapeutic window, allocation concealment, blinded assessment of outcome, multiple endpoints for both immunohistological and behavioral outcomes, study of outcomes for more than 3 weeks after stroke onset, and reporting of potential conflicts of interest and study funding [50].

2.6. Endothelin-1 stroke

Stroke surgeries were carried out as described previously [51,52]. Anteroposterior (AP) and mediolateral (ML) coordinates are measured relative to bregma; dorsoventral (DV) coordinates are relative to the skull surface. Rats were anesthetized with isoflurane, shaved and placed into a Kopf stereotaxic instrument. An off-midline incision was made in the scalp and a 2.7 mm burr hole, centered at AP +1.15 mm and ML +3.0 mm, was made using a trephine drill bit (Cat.# 18004–27, *Fine Science Tools Inc*, Vancouver, BC, Canada). Et-1 (400 pmol/μL in ddH2O, ab120471, *Abcam*, Cambridge, MA, USA) was injected using a 10 μL Hamilton syringe with a 26G, 45° bevel needle (Model 1701 RN, Hamilton) controlled with an automated injector (Pump 11 Elite Nanomite, *Harvard Apparatus*, Saint-Laurent, QC, Canada). Injections were made into the following coordinates in the motor cortex and in the striatum: motor cortex 1) AP + 2.3, ML ± 3.0 mm, DV -2.3 mm; motor cortex 2) AP 0 mm, ML ± 3.0 mm, DV -2.3 mm; striatum 3) AP 0.7 mm, ML ± 3.8 mm, DV -7.0 mm.

For each injection, the needle was lowered to 0.1 mm past its DV coordinate (i.e. −2.4 mm DV) and then raised +0.1 mm to its final DV position (i.e. −2.3 mm DV). The needle was left to equilibrate for 1 min, after which 1 μL Et-1 was injected at 0.25 μL/min over 4 min. After injection, the needle was left for an additional 2 min and then slowly withdrawn. After completing Et-1 injections, a 2.5 mm silicone disk was placed on the exposed dura surface, the cranial defect was filled with gelfoam (Spongostan Standard, MS0002, *Ethicon*, New Jersey, USA) and sealed with bone cement (Ortho-Jet BCA, *Lang Dental*, Illinois, USA), and the skin was sutured closed. The silicone disks were made by punching out a 2.5 mm hole from medical grade silicone sheets (Medical Grade Silicone Sheeting, CUST-20001-005, *BioPlexus*, California, USA) using a 2.5 mm biopsy punch (Cat. 33-31 B, *Miltex*, Pennsylvania, USA) and then autoclave sterilized.

2.7. Gel implantation

Four days after the stroke surgery animals received a second surgery for HAMC gel injection. The following were removed from the first surgery: bone cement sealant covering the cranial defect, the gel foam and the silicone sheet. The dura underlying the cranial defect was surgically resected with the aid of a surgical microscope, taking care not to remove the pial vessel layer. A curved 5.9 mm polycarbonate disk (Fig. 1A, top) [10], with a 2.7 mm opening, was fixed over the burr hole with bone glue (Loctite 454, *Henkel Corporation*, Rocky Hill, CT, USA), as previously described [6]. Six μL of HAMC gel with (or without) PLGA microparticles were directly injected onto the brain's cortical surface, filling the space formed by the skull and disk (Fig. 1A, top). A second 5.9 mm polycarbonate disk with no opening was placed over top of the first disk and the skin was sutured closed.

Untreated control (Sham) animals received identical procedures (stroke, durectomy and drug delivery casing installation) but had no gel injected onto the brain. Rather, a 2.7 mm silicone disk was placed onto the surface of the brain after the durectomy and the space otherwise occupied by HAMC was filled with gelfoam wetted with PBS. The polycarbonate disk system was installed in the same manner as done for HAMC treated animals.

2.8. Analysis of CsA and EPO concentration in the brain

To measure CsA and EPO concentrations in the brain after local delivery, Sprague Dawley rats (29 male, 300–350 g) were given the Et-1 stroke injury followed by HAMC gel implantation with both CsA and EPO PLGA microparticles 4 d later. The ipsilateral brain tissue was harvested at terminal time points (5, 10, 20, 32 and 46 days after stroke), snap frozen whole and stored at −80 °C. Once tissue had been collected from all time points, all tissue sections were simultaneously prepared for depth vs. concentration analysis, as previously described [6]. Briefly, six coronal sections surrounding the stroke lesion, each 1-mm thick, were cut out using a McIlwain tissue chopper (*Mickle Laboratory Engineering Company*, Surrey, UK) and dorsoventral sections, each 0.5 mm thick, were collected from the coronal slices using a Leica CM3050S cryostat system; sections at the same were combined in 2 mL polystyrene microtubes. Tubes were weighed before and after sample collection to determine the mass of brain tissue collected.

Tissue was homogenized for 1.5 min with a Mini-beadbeater 16 (*Biospec Products, Bartlesville, OK, USA*), cooled on ice for 1.5 min, and homogenized again for 1.5 min. Before tissue homogenization, 5 × 1.0-mm diameter zirconia beads (Cat.#11079110zx, *Biospec Products*), 200 μL of 325 mM $ZnSO_4$ with 0.1% glycerol and 50 μL of methanol (MeOH, HPLC grade, *Caledon Labs*, Georgetown, CA, USA) containing 25 ng/mL FK-506 (F-4900, LC Laboratories). The $ZnSO_4$ served as a chelating agent, the glycerol served to protect drugs during homogenization and the methanol with FK-506 (IS) served as an internal control for CsA analysis. After homogenization 100 μL of homogenate was separated for CsA concentration analysis and 100 μL of homogenate was separated for EPO concentration analysis.

For CsA analysis, CsA was extracted by adding 150 μL acetonitrile (ACN, HPLC grade, *Caledon Labs*), homogenizing tissue for 1 min, centrifuging at 4 °C for 10 min at 16,000 G and removing the supernatant for analysis. CsA was detected by high pressure liquid chromatography tandem mass spectrometry (HPLC-MS/MS), as described previously [13]. CsA standards in MeOH with IS (final assay concentration: 0.25–100 ng/mL) were spiked in stroke-injured brain tissue that received a vehicle gel (HAMC + 20 wt/vol% PLGA) that were exacted through the same extraction procedure. The amount of CsA at each depth was divided by the mass of brain tissue to determine the concentration in the brain as micrograms of CsA per gram of brain tissue.

For EPO analysis, the homogenate was diluted with 100 μL of EPO ELISA diluent, vortexed for 10 s and centrifuged at 4 °C for 10 min at 16,000 G. 100 μL of supernatant was analyzed for EPO concentration using an ELISA kit (Human Erythropoietin Quantakine ELISA kit, DEP00, *R&D systems*). EPO standards were spiked in stroke-injured brain tisue that received a vehicle gel (HAMC + 20 wt/vol% PLGA) that were exacted through the same extraction procedure (final assay concentration 21–3360 pg/mL). The amount of EPO at each depth was divided by the mass of brain tissue to determine the concentration in the brain as nanograms of EPO per gram of brain tissue.

2.9. Analysis of CsA concentration in the peripheral blood

We used CsA as a model compound to measure the amount of drug in the peripheral blood after local delivery with HAMC, and to compare local drug delivery with HAMC against systemic drug delivery with subcutaneously implanted osmotic minipumps. Given EPO's limited transport across the blood-brain barrier [53], we assumed that EPO concentration in the peripheral blood after local delivery would be similar to, or lower than, that of CsA.

The experiments were performed on Long Evans rats (10 male, 350–425 g) due to animal availability. Stroke surgeries were carried out as above. At the time of injury, animals were implanted with either

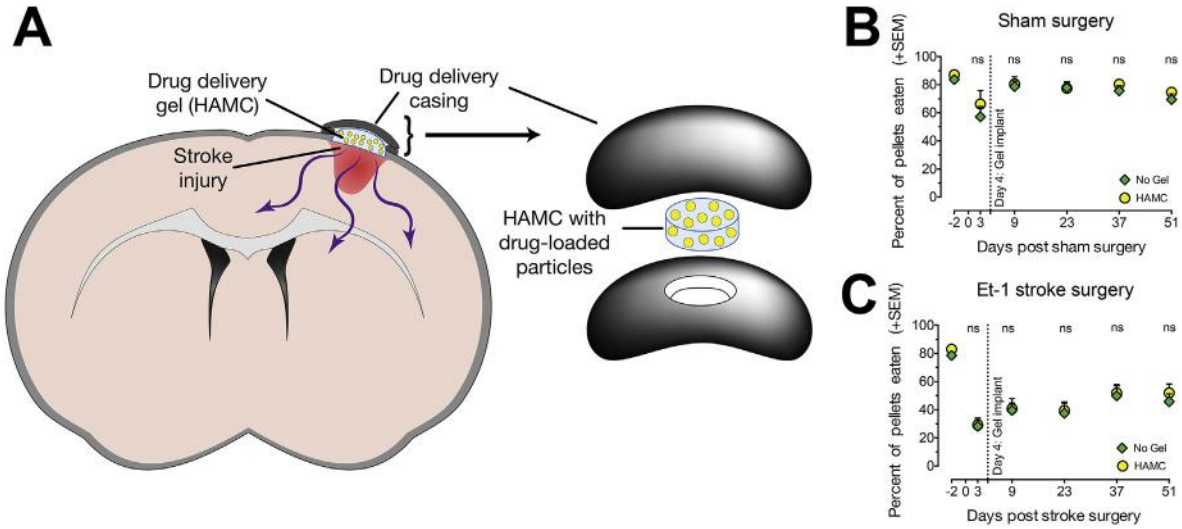

Fig. 1. Epi-cortical HAMC implant for local drug delivery. (A) Schematic of the epi-cortical local drug delivery system. A hyaluronan and methylcellulose (HAMC) hydrogel was injected onto the surface of the brain after a craniotomy and enclosed in polycarbonate casing, thereby serving as a depot for local drug release. Sustained drug release was achieved by encapsulating drugs in degradable polymeric particles and suspending them inside the gel. (B, C) Motor function after epi-cortical implant of a blank (drug-free) HAMC gel was evaluated in uninjured ("Sham surgery", craniotomy-only) and Et-1 stroke-injured rats, and compared to a sham implant (No Gel). (B) Uninjured animals show no sustained deficits after epi-cortical HAMC implantation relative to controls with no gel (No Gel, n = 7 rats; HAMC, n = 6). (C) Stroke surgery produces a sustained deficit (No Gel, n = 7 rats; HAMC, n = 8). Importantly, HAMC does not cause any further functional deficit and is equivalent to the No Gel treatment. Data are expressed as mean + s.e.m and all data points represent individual rats. In (B) and (C), ns, not significant by two-way ANOVA (Time x Treatment Group) with Bonferroni's multiple comparison test (5 comparisons).

HAMC hydrogel with CsA microparticles, as described above, or an osmotic minipump. A 14-day, 0.425 μL/h minipump (Alzet Model 2002, *Durect Corporation,* Cupertino, CA, USA) loaded with 425 mg/mL CsA in conventional 65% ethanol and 35% cremaphor was inserted into a small incision made over the right shoulder. The minipump was inserted into the subcutaneous space, with the minipump's opening facing away from the incision, and the incision was sutured closed. To keep the cranial defect sealed in these animals a 5.9 mm polycarbonate disk with no opening was fixed over the burrhole.

At 7 days post-stroke, the rats were sacrificed and whole blood was collected in 2 mL polystyrene microtubes that were pre-weighed; the tubes were weighed again after blood collection to determine sample mass before freezing and storing at −80 °C. An additional Long Evans rat that did not receive any drug was also sacrificed and its blood collected to serve as a clean blood control. Approximately 0.4 g (400 μL) or of whole blood was collected per animal.

When the samples were to be processed, 20 × 1.0-mm diameter zirconia beads, 200 μL of 325 mM $ZnSO_4$ and 200 μL MeOH containing 25 ng/mL FK-506 (IS), as an internal control, were added to the tubes. The samples were homogenized for 1.5 min, cooled on ice for 1.5 min, and homogenized again for 1.5 min. Then, 400 μL of homogenate was added to 600 μL of ACN and homogenized for 1 min to extract CsA. The sample was then centrifuged at 4 °C for 15 min at 16,000 G and the supernatant was removed for analysis. Systemic delivery samples were diluted 10X in a medium matching the supernatant (60% ACN, 20% saline, 20% 325 mM $ZnSO_4$ and 20% MeOH with 25 ng/mL FK-506). Local delivery samples were undiluted. CsA standards in MeOH with FK-506 were exacted through the same extraction procedure. The standard curve ranged from 0.25 to 50 ng/mL. Whole blood from the rat that did not receive any drug was also processed in the same manner and used to set a lower limit of signal detection. All the collected supernatants and standards were analyzed with HPLC-MS/MS, as described previously [13].

2.10. Behavioral training and testing

The cylinder and Montoya staircase tasks were used to measure forelimb function [54,55] in Sprague Dawley rats (148 male, 225–275 g). In the Montoya staircase task animals were trained to retrieve pellets from a staircase apparatus using both paws; a total of 21 pellets were available to each paw. Training was done twice a day for a minimum of 14 consecutive days prior to stroke injury. Baseline performance was calculated as the average of the animal's performance on the last 4 trials of training, during the 2 days prior to stroke injury. Animals were successfully trained, and thus included in the staircase analysis, if their baseline score was 15 pellets or greater; if animals were successful with both paws, the paw with the higher average was targeted with the stroke; if both paws had the same average score, then the paw with a lower standard deviation during the last 4 trials was chosen. The scores were expressed as a percentage of the maximum number of pellets available (i.e. 21). At day 3 post-stroke animals were tested 3 times on the staircase to obtain an estimate of the stroke deficit; the last 2 trials were averaged to obtain a measure of the stroke deficit. The deficit was calculated as the score on day 3 as a percentage of the baseline score (i.e. day 3/baseline). Animals were grouped into large deficit (< 20% of baseline performance), medium deficit (20–65% of baseline performance), minimal deficit (65–85% of baseline performance) and no deficit (> 85% of baseline performance). These groups were used to distribute the animals to the 5 treatment groups in a balanced and randomized manner. After gel implantation the animals were tested over time. For each time points the animals were tested across 3 days, 2 tests per day (e.g. on days 8, 9, and 10 for day 10 time point). The last 4 trials (e.g. from days 9 and 10) were averaged to obtain their staircase performance. Animals were included in the analysis if their day 3 deficit score was less than 65% of baseline performance, indicating a sufficient deficit in the staircase task. The experimenter was blinded to the animals treatment group and injured hemisphere.

In the cylinder task animals were tested once before stroke surgery (baseline measurement), once at day 3 (post-stroke pre-implant measurement), and once at each post-implantation time point. Animals were placed in a plexiglass cylinder (20 cm inner diameter, 36 cm height) situated atop a clear plexiglass surface. Animals were recorded from underneath as they explored the cylinder until they made a minimum of 15–20 rears. A rear was defined as an animal standing up on its hindpaws, with both forepaws disengaged from the ground, and

touching the wall of the cylinder with at least one forepaw. The rear is complete when the animal returns to the ground on all 4 paws. The experimenter was blinded to the animals treatment group and injured hemisphere. Later, two scorers independently scored the animals; both scorers were blind to the animal's experimental group and stroke hemisphere. Scoring was done to assess the number of times the animal touched the cylinder wall with it's injured limb while reared on it's hindpaws; multiple touches may occur in a single rear. Animal's paw use was calculated as:

$$\%\ injured\ paw\ use = \frac{unilateral\ injured\ paw\ touches\ +\ (0.5\ \times\ bilateral\ paw\ touches)}{unilateral\ injured\ paw\ touches\ +\ bilateral\ paw\ touches\ +\ unilateral\ uninjured\ paw\ touches}$$

$$\%\ pre\text{–}stroke\ paw\ use = \frac{\%\ injured\ paw\ use}{\%\ to\ -\ be\ -\ injured\ paw\ use\ before\ stroke}$$

Touches were scored as unilateral (left or right hand) and bilateral; assessment of which paw was counted as the injured paw was done post-hoc. A touch was defined as a weight-bearing wall contact with 3 or 4 fingers and the palm of the hand. A 3-finger contact was counted if it appeared to involve weight-bearing, as indicated by the movement of the animal and finger flexion. Touches were counted during the upward motion of the rear and during full rearing; touches during the downward motion of the rear were omitted. Multiple touches were only counted if a paw is fully removed and replaced (during a unilateral touch) or both paws are removed and one or both paws are replaced (during a bilateral touch). Scores of animal's %-injured paw use were averaged between the two scorers; discrepancies greater than 20% were re-scored. The % pre-stroke paw use was calculated based on the average of the two scorers. Animals were included in the analysis if their % pre-stroke paw use at day 3 was less than 70% of baseline (indicating the animal had a sufficient deficit in the cylinder task) but greater than 30% baseline (indicating the deficit wasn't too great for recovery).

2.11. Brain tissue preparation for histological analysis

Sprague Dawley rats (male, 225–275 g) used for immunohistochemistry were transcardially perfused with saline followed by 4% paraformaldehyde. A total of 103 rats were used: 55 rats for day 4 and day 10 tissue and 48 rats, taken from behavioral studies, for day 46 tissue. Brains were extracted and fixed in 4% paraformaldehyde at 4 °C overnight, followed by cryoprotection in 15% and then 30% sucrose. Cryoprotected brains were snap frozen and coronal sections cryosectioned at 30 μm slice thickness.

2.12. Immunohistochemistry

Sections were permeabilized for 30 min (1% Triton X-100 in PBS), blocked for 30 min (0.1% Triton X-100 and 5% BSA in PBS) and incubated in primary antibodies, diluted in blocking solution (dilutions specific to each antibody), overnight at 4 °C. Sections were then washed 3 times, 5 min each time, in PBS and incubated in secondary antibodies and DAPI (1 μg/mL final concentration, D1306, *Invitrogen Inc.*, Burlington, ON, Canada), both diluted in blocking solution, for 1 h at 25 °C. Sections were washed 3 times in PBS and mounted with Fluorogold (Cat.#1887462, *Invitrogen Inc.*) mounting media.

The primary antibodies used (final concentration or dilution listed) were: rabbit anti-NeuN (0.395 μg/mL, ab177487, *Abcam*) for day 46 tissue, chicken anti-NeuN (0.1 μg/mL, ABN91, *EMD Millipore*, Billerica, MA, USA) for NeuN for day 4 and day 10 tissue, rabbit anti-Sox2 (1:500, ab59776, *Abcam*), mouse anti-Ki67 (0.25 μg/mL, Cat.#550609, *BD Pharmingen*, Mississauga, ON, Canada), rabbit anti-DCX (0.25 μg/mL, ab18723, *Abcam*), and rabbit anti-synaptophysin (0.574 μg/mL, ab32127, *Abcam*). The rabbit anti-NeuN could not be used on the day 4 and day 10 tissues because they were co-stained with rabbit anti-synaptophysin. Thus, it was necessary to use chicken anti-NeuN at day 4 and day 10.

All secondary antibodies were highly cross-absorbed variants, where available, to minimize background fluorescence. The secondary antibodies used (final concentration listed) were: AlexaFluor 488 goat anti-mouse (2 μg/mL, Cat.#A-11029, *Invitrogen Inc.*) for Ki67, AlexaFluor 488 goat anti-rabbit (2 μg/mL, Cat.#A-11034, *Invitrogen Inc.*) for DCX and synaptophysin, AlexaFluor 546 goat anti-rabbit (2 μg/mL, Cat.#A-11035, *Invitrogen Inc.*) for Sox2, AlexaFluor 633 goat anti-rabbit (2 μg/mL, Cat.#A-21071) for NeuN ab177487, AlexaFluor 633 goat anti-chicken (2 μg/mL, Cat.#A-21103, *Invitrogen Inc.*) for NeuN ABN91.

2.13. Lesion volume measurement

Coronal $NeuN^+$ stained sections spaced 300–600 μm apart from AP +5 mm to AP -3.0 mm (relative to bregma) were assessed for stroke lesion size. A total of 6–12 sections were assessed per animal, depending on the lesion size. Images were captured using a Zeiss AxioScan.Z1 slide scanner at 10x magnification with a resolution of 1.5314 μm/pixel.

The stroke cavity area in each section was defined as the loss of tissue ($DAPI^-$) and quantified as the difference in the $DAPI^+$ contralesional and ipsilesional hemisphere area. The stroke infarct area was defined as the area lacking regular $NeuN^+$ staining ($DAPI^+$ and $NeuN^-$) in the ipsilateral hemisphere, using the contralateral hemisphere as a reference; the cortical and striatal infarct volumes were separately measured. The area in each section was measured using Fiji (ImageJ) software [56] and the volume between sections was calculated using the average cavity or infarct area between sections multiplied by the inter-section distance. The total cavity and infarct volumes were calculated by summing the individual volumes between sections. The lesion volume is the sum of the cavity, the cortical infarct and the striatal infarct. The experimenter was blinded to the animals treatment group during analysis.

2.14. Neural stem cell quantification

The number of $Sox2^+$ and $Ki67^+$ pixels in the lateral ventricles of the ipsilateral and contralateral hemispheres was counted in 3 coronal sections located at approximately: AP +0.6, 0.0, and −0.6 mm, relative to bregma. The lateral ventricles, home to neural stem cells in the adult forebrain [57,58], were identified anatomically in images by their location and shape using $DAPI^+$ staining. Images were captured using a Zeiss AxioScan.Z1 slide scanner at 10x magnification with a resolution of 1.5314 μm/pixel. DAPI staining was used to identify and isolate the dorsoventral walls of the ventricles in Fiji software. The “Intermodes” threshold algorithm was used to set $Ki67^+$ pixels to white and $Ki67^-$ pixels to black. The “Otsu” threshold algorithm was used to set $Sox2^+$ pixels to white and $Sox2^-$ pixels to black. The thresholded Ki67 and Sox2 images were merged to determine the overlapping pixels. The total number of white pixels in each set of images (Ki67, Sox2 and Ki67 + Sox2 overlap) along the dorsoventral walls was counted using Fiji. The experimenter was blinded to the animals treatment group during analysis.

Pixel counts were converted to cells by calculating the average number of pixels per cell in 10 ventricle sections. The cells within a region were manually counted along with the number of corresponding pixels for each of Ki67, Sox2 and Ki67 + Sox2 overlap. From this a pixel-to-cell ratio was calculated for Ki67 (67.38 pixels/cell), Sox2 (72.14 pixels/cell), and Ki67 + Sox2 (61.64 pixels/cell).

2.15. Synaptophysin density quantification

The density of synaptophysin$^+$ puncta in the peri-infarct was quantified in circular ROI's with a 0.25 mm diameter, evenly located around the infarct border. As the sections were co-stained with NeuN, the NeuN$^-$ border was used to demarcate the beginning of the peri-infarct. A total of 6–12 sections were assessed per animal, depending on the lesion size. These were quantified in the 0–0.25 mm range from the infarct border. The ROIs were processed with a high pass filter by using the "Sharpen" function twice on Fiji. The processed ROI's were then converted to set synaptophysin$^+$ pixels to white and synaptophysin$^-$ pixels to black using the "Moments" threshold algorithm. The number of positive pixels was counted and expressed as a density. The experimenter was blinded to the animals treatment group during analysis.

In the contralesional hemisphere, the thickness of the cortical layer was measured and used to estimate the location of layer ii/iii. Layer ii/iii was 10–30% of the cortical thickness. In the striatum circular ROIs, whose thickness depended on the span of the striatum, were used to quantify the lateral region of the striatum. The span of the striatum was measured as the length from the dorsolateral extrema to the ventromedial extrema of the striatum. The lateral striatum ROI was 12.5% the span of the striatum. The ROI's for the lateral region were placed bordering the corpus callosum (0–12.5% the striatum span from the corpus callosum). The same method was used to quantify the synaptophysin$^+$ puncta density in the ROIs. A total of 4–10 sections were assessed per animal. The experimenter was blinded to the animals treatment group during analysis.

2.16. Migratory neural progenitor cell count

The number of migratory DCX cells located in the stroke penumbra, corpus callosum and striatum and corpus callosum were manually counted on a fluorescence microscope using a 20X objective lens. Four coronal sections were countered per brain and were centered around the lesion. All counts were performed in a blinded fashion. Cells were only counted if they were co-localized with DAPI nuclear staining and were clearly located outside the tightly clustered population of cells along the ventricles. Thus, the population of cells counted did not overlap with the population of cells quantified by the pixel counts. The experimenter was blinded to the animals treatment group during analysis.

2.17. Statistics

Results are reported as mean + standard error of the mean. Statistical analyses were performed using Prism6.0 (*GraphPad Software Inc.*). Multiple comparisons between groups were performed using a one-way ANOVA or two-way ANOVA, with the Dunnett or Bonferroni post-hoc tests. For factorial design experiments (NSPC number, proliferating NSPCs, migrating neural progenitors and synaptophysin puncta), a two-way ANOVA was used to assess the significance of treatment main effects and any interactions between the two drug treatments. Reported p-values are adjusted for multiple comparisons, where appropriate.

3. Results

3.1. Motor recovery is improved and accelerated by combined delivery of CsA and EPO

We formulated a modular delivery system to release CsA and EPO to the stroke-injured rat brain for at least 4 weeks post-implant using drug-loaded PLGA microparticles dispersed within the HAMC gel. The gel was implanted onto the surface of the rat brain, 4 days after injury, to avoid the tissue damage that typically occurs from intracranial implants. The composite was enclosed in a polycarbonate casing and sealed with dental cement to avoid any drug leakage to the cerebrospinal fluid (CSF) (Fig. 1A).

To ensure that the method itself did not cause further injury to the brain, we first evaluated behavioral function in both healthy and stroke-injured rats after depositing a drug-free HAMC hydrogel. Using the Montoya staircase behavioral assay, which is sensitive to deficits in fine motor function [54], we demonstrated that HAMC deposition onto the brain of healthy adult rats produced no sustained deficits (Fig. 1B). To investigate its application in the injured brain, we used the endothelin-1 transient ischemia model in Sprague Dawley rats, inducing stroke injuries in the cortex and striatum to produce sustained motor deficits. Implanting HAMC onto the surface of the brain 4 days after the stroke-injury did not interfere with motor function after stroke compared to an injury-only control (Fig. 1C). Given the innocuousness of our delivery platform, we then investigated its use for local, sustained drug release to the brain.

Functional recovery after stroke relies on mechanisms underlying neural plasticity [59], such as promoting cell survival, neurogenesis and neural connectivity, among others. We hypothesized that the combination of locally delivered CsA and EPO would produce greater functional recovery than either drug alone by stimulating multiple repair pathways. CsA and EPO were each encapsulated in separate PLGA particles and then combined into the HAMC hydrogel. The concentration of PLGA was kept constant (20% w/v) in all groups including in controls where we included blank CsA-formulated single emulsion particles or blank EPO-formulated double emulsion particles or both. The following groups were compared: CsA + EPO (10% w/v CsA particles + 10% w/v EPO particles), vehicle (10% w/v *blank*-single emulsion particles + 10% w/v *blank*-double emulsion particles), CsA-alone (10% w/v CsA particles + 10% w/v *blank*-double emulsion particles), EPO-alone (10% w/v EPO particles + 10% w/v *blank*-single emulsion particles). On day 4 after stroke, the drug-infused HAMC/PLGA composite was deposited directly on the cortex and then recovery in gross and fine motor function was assessed for 6 weeks using cylinder and staircase tasks.

The cylinder task assesses recovery of spontaneous forelimb use during exploratory behavior; recovery in this task is indicative of motor and sensory function repair [54]. All groups dropped to ~50% of pre-stroke paw use at day 3, demonstrating a functional deficit of the Et-1 injury (Fig. 2A). CsA + EPO treatment resulted in greater recovery in the cylinder task, with significant improvement at day 10 ($p < 0.05$ vs. CsA-alone) and day 20 ($p < 0.05$ vs. vehicle, CsA-alone and EPO-alone) (Fig. 2B); however, no significant differences between groups were found at days 32 and 46. Neither vehicle nor single-drug treated groups recovered over time compared to pre-implant testing at day 3 (Supplemental Figs. 1A–C). Combined CsA + EPO treatment had a synergistic effect, as animals showed a significant improvement by day 20 not seen with either drug alone; this effect was maintained out to day 46 (Supplemental Fig. 1D).

The staircase task assesses recovery of skilled forelimb use; recovery in this task is indicative of fine motor functional repair. All groups dropped from 80% success rate in pellet retrieval before injury to 25% at day 3 after injury, reflecting a functional deficit of the Et-1 injury (Fig. 2C). CsA + EPO treatment accelerated recovery in the staircase task, with significant improvements over controls at days 10 and 20 ($p < 0.05$ vs. vehicle) (Fig. 2D); yet, no improvement was seen relative to single-drug treatment. No significant differences between groups were found at days 32 and 46. The vehicle, CsA-alone and EPO-alone groups improved significantly at day 10 relative to day 3, to an average of 40% success on the task (Supplemental Figs. 2A–C). Only the CsA + EPO treated animals clearly demonstrated accelerated recovery with a 60% success rate at day 10 (Supplemental Fig. 2D), which was not matched by other groups until days 32–46.

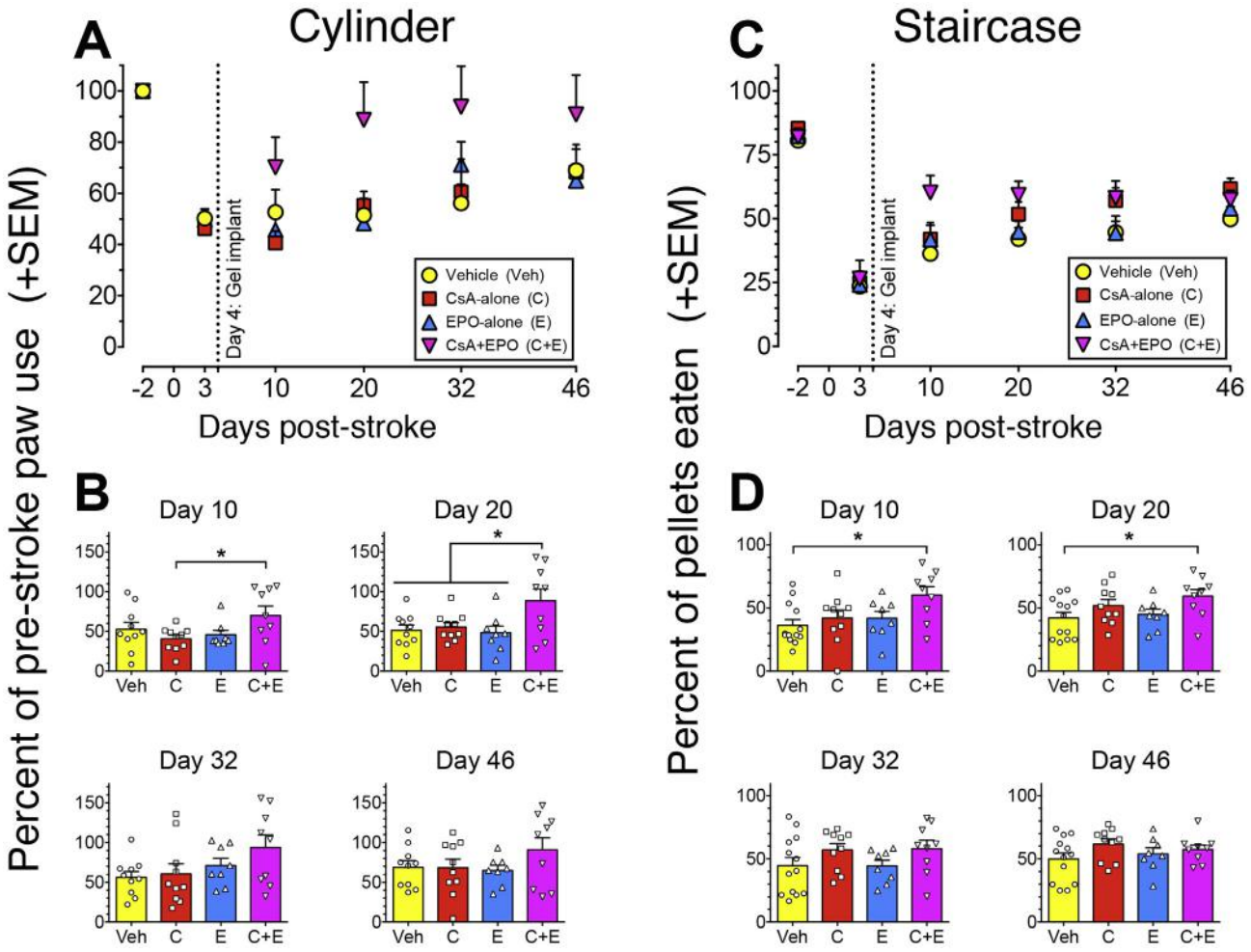

Fig. 2. Motor recovery is increased by combined delivery of CsA and EPO. (A, B) Quantification of animal functional recovery in the cylinder task, expressed as injured paw use relative to pre-injury conditions. **(B)** Shows the comparisons of recovery in the cylinder task from (A), demonstrating significant improvement with CsA + EPO treatment at days 10 and 20 (vehicle, n = 10 rats; CsA-alone, n = 10; EPO-alone, n = 8; CsA + EPO, n = 9). **(C, D)** Quantification of animal performance in the staircase task, expressed as % success in the task. **(D)** Shows the comparisons of recovery in the staircase task from (C), demonstrating significant improvement with CsA + EPO treatment at days 10 and 20 (vehicle, n = 13 rats; CsA-alone, n = 10; EPO-alone, n = 8; CsA + EPO, n = 9). Data are expressed as mean + s.e.m and all data points represent individual rats. Significance was evaluated at each time-point by a one-way ANOVA with Dunnett's post-hoc test vs. CsA + EPO (3 comparisons); *p < 0.05.

3.2. Epi-cortical drug delivery from HAMC-PLGA composite provides sustained release

Since recovery plateaus after day 20 post-stroke in animals treated with CsA + EPO (Fig. 2), we wondered if drug release also ceases after day 20. To answer this question, we measured CsA and EPO concentrations in the brain following a similar paradigm to the behavioral recovery experiments. We implanted the HAMC-PLGA gel 4 days after stroke and measured local drug release at 5, 10, 20, 32 and 46 days post-stroke, corresponding to 1, 6, 16, 28 and 42 days post-implant. We obtained the average concentration and spatial distribution of each drug in the ipsilesional hemisphere by analyzing the drug concentrations in serial dorsoventral sections starting from the brain surface and going down to 6 mm deep, thereby including the subventricular zone of the lateral ventricles where the neural stem cells are found.

Drug release from the HAMC-PLGA is immediate and sustained, as CsA and EPO each diffused into the brain within the first day post-implant and were found in the brain for at least 32 (but not 46) days post-stroke (Fig. 3A). Although no drug was found in the brain at 46 days post-stroke, we observed PLGA particles in the implant site at this time point. The highest concentrations were seen within the first 6 days post-implant, during which recovery is greatest in the staircase and cylinder tasks (Fig. 2). This resulted primarily from direct transport into the brain from the HAMC-PLGA implant and not vascular transport: using CsA as a representative compound, we demonstrated that drug concentrations in the peripheral blood were very low with HAMC delivery (Supplemental Fig. 3). Importantly, both drugs diffuse through the injured brain and reach the sub-cortical NSPC niche, located 2.5–4.5 mm below the brain surface (Fig. 3B), within the first day post-implant. Thus, CsA and EPO were locally delivered to the stroke-injured rat brain for up to 32 days post-stroke (or 28 days post-implant) where they acted on host brain tissue during both acute and chronic stages of injury to promote recovery.

3.3. EPO treatment increases the number of NSPCs and migrating neuroblasts

Few studies that investigate drug combinations have been done systematically to differentiate the individual effects of each drug. Using factorial design, we isolated the individual effects of each drug on endogenous repair and tested whether any additive effect existed between the two drugs using a two-way ANOVA (CsA x EPO) (Fig. 4A). This was evaluated on day 10 post-stroke, the time point at which CsA + EPO animals recovered significantly in both staircase and cylinder tasks.

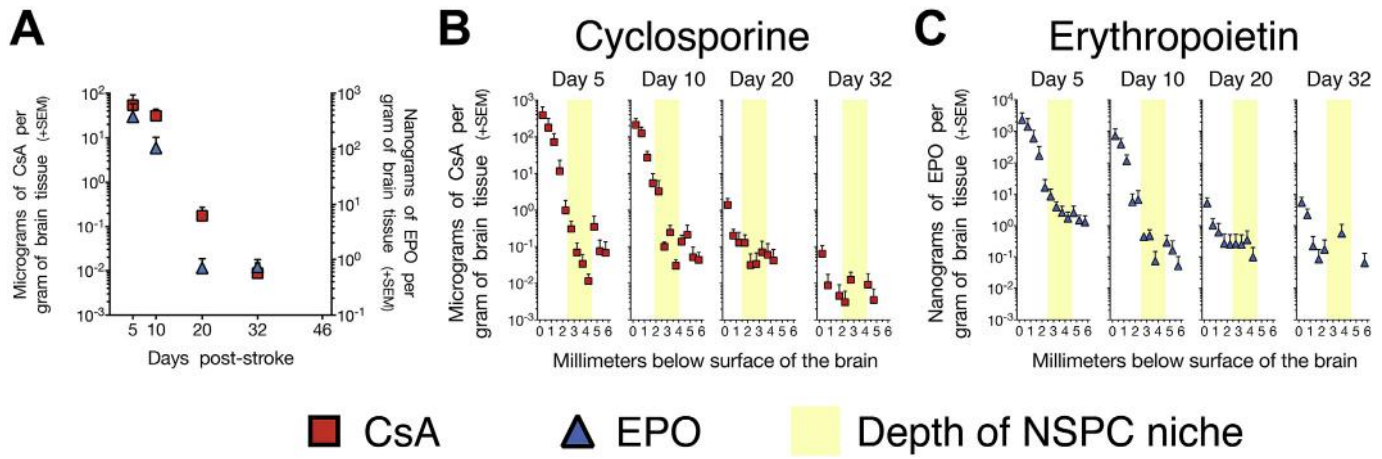

Fig. 3. Local drug delivery with HAMC provides sustained release to the stroke-injured rat brain. (A) Quantification of average CsA and EPO concentration in the ipsilesional hemisphere over time after implanting a gel with 10% w/v CsA particles and 10% w/v EPO particles at day 4 post-stroke demonstrate sustained release and accumulation in the rat brain for at least 32 days. **(B, C)** Analyses of the spatial distribution of (B) CsA and (C) EPO as a function of depth from the brain surface revealed that both drugs diffused to the depth of the periventricular NSPC niche (highlighted, yellow). Data are expressed as mean + s.e.m and all data points represent individual rats. In (A), (B) and (C), n = 5 rats, except day 5 where n = 4 rats. (For interpretation of the references to colour in this figure legend, the reader is referred to the Web version of this article.)

We first determined the drug effects on the number of $Sox2^+$ NSPCs in the lateral ventricles of the forebrain stem cell niche, since both CsA and EPO are known to stimulate NSPCs (Fig. 4B; Supplemental Fig. 4). Only EPO treatment (EPO alone or CsA + EPO) significantly increased the number of NSPCs in the ipsilesional ventricles ($F_{1,28}$ = 4.61, p = 0.041) (Fig. 4C and D), in the absence of any effect on NSPC proliferation ($F_{1,22}$ = 0.032, p = 0.86) (Fig. 4E and F). No effect was seen with CsA treatment on total NSPC number ($F_{1,28}$ = 0.75, p = 0.40) or proliferating NSPCs ($F_{1,22}$ = 0.041, p = 0.84). No interaction effect between CsA and EPO was found for total NSPC number ($F_{1,28}$ = 0.77, p = 0.39) or proliferating NSPCs ($F_{1,22}$ = 0.35, p = 0.56). Neither drug affected NSPCs in the contralesional ventricles.

We then assessed the effect of CsA and EPO on migrating neuroblasts by counting DCX^+ neuroblasts located outside of the lateral ventricles, in the corpus callosum, striatum and injured cortex (Fig. 4G; Supplemental Fig. 5). EPO significantly increased the number of migratory neural progenitors located outside the ventricular niche ($F_{1,23}$ = 4.56, p = 0.044); no effect was seen with CsA ($F_{1,23}$ = 0.40, p = 0.53) (Fig. 4H and I). No interaction effect between CsA and EPO was found ($F_{1,23}$ = 0.0015, p = 0.97). Neither CsA nor EPO had an effect in the contralesional hemisphere, but EPO-treated groups had a similar trend toward increased numbers of migrating neural progenitors.

3.4. Synaptic plasticity is differentially affected by CsA and EPO

Since we observed functional recovery at an early, 10-day time point with co-delivery of CsA and EPO, we hypothesized that changes in synaptic plasticity, and not neuronal replacement, were contributing to this early recovery. To test this hypothesis, we measured the effects of CsA and EPO on synaptic plasticity by quantifying the density of synaptophysin$^+$ vesicles in the ipsilesional and contralesional hemispheres (Fig. 5A) at day 10 post-stroke. In the ipsilesional hemisphere we measured synaptic plasticity in the peri-infarct, a 250 μm region adjacent to the infarct border, which was demarcated by $NeuN^-$ cells. As there was no peri-infarct in the contralesional hemisphere we defined regions of interest to measure synaptophysin$^+$ vesicle density, which were applied uniformly across all tissue sections analyzed. In the contralesional cortex we measured synaptophysin density in layers ii/iii, which contain cross-hemispheric projections, and v/vi, which contain corticospinal projections. In the contralesional striatum we measured synaptophysin density in a lateral region bordering the corpus callosum and in an adjacent region located medially. In each region (Fig. 5B–G) we used a factorial design and two-way ANOVA (CsA x EPO) to determine the effect of each drug, and the presence of any interactions, on synaptophysin density, as illustrated in Fig. 4A.

CsA and EPO both affected synaptophysin vesicle density, though in different ways (Supplemental Fig. 6). In the cortex EPO significantly decreased vesicle density in the contralesional cortex, specifically in cortical layers ii/iii (Fig. 5B), as determined by a two-way ANOVA ($F_{1,28}$ = 4.82, p = 0.037). In the striatum CsA increased synaptophysin$^+$ vesicles in both the striatal peri-infarct ($F_{1,28}$ = 5.813, p = 0.023) and the contralesional striatum ($F_{1,28}$ = 4.61, p = 0.041). Neither drug had a significant effect on synaptophysin$^+$ vesicles in the cortical peri-infarct. No interaction effect was observed in any region (p > 0.05).

3.5. Stroke lesion volume is decreased by combined delivery

To examine the effect of CsA and EPO co-delivery on cell survival and tissue repair, we compared the stroke lesion volume at 3 time points: day 4 (sub-acute, prior to epi-cortical implant), day 10 (sub-acute) and day 46 post-stroke (chronic). The lesion volume was calculated as the sum of the stroke cavity ($DAPI^-$ volume) and stroke infarct ($DAPI^+$ $NeuN^-$ volume) in both cortex and striatum (Fig. 6A).

The lesion volume progressively decreased with time after CsA + EPO treatment ($F_{2,23}$ = 3.349, p = 0.053) and was significantly smaller at day 46 vs. day 4 (p < 0.05) (Fig. 6B); the effect appeared to be additive, consistent with previous reports of tissue repair [38]. In single-drug treated groups, the lesion volume did not decrease significantly with time; the decrease in infarct volume was balanced by the increase in cavity volume likely due to the clearance of dead tissue as part of the natural injury response (Supplemental Fig. 7). As a result, the overall stroke lesion volume did not change in these groups and was similar to the untreated, stroke-injured brain.

The data demonstrated that tissue repair was achieved only with CsA + EPO co-delivery. Relative to the vehicle control at day 46, CsA-alone reduced the lesion volume by 23% while EPO-alone reduced the lesion volume by 27%. Treatment with CsA + EPO reduced the lesion volume by 50%, relative to the vehicle at day 46, which was equivalent to the sum of CsA-alone and EPO-alone groups (50%), suggesting that the drugs had an additive effect on stroke lesion volume and impacted independent mechanisms within the injured tissue.

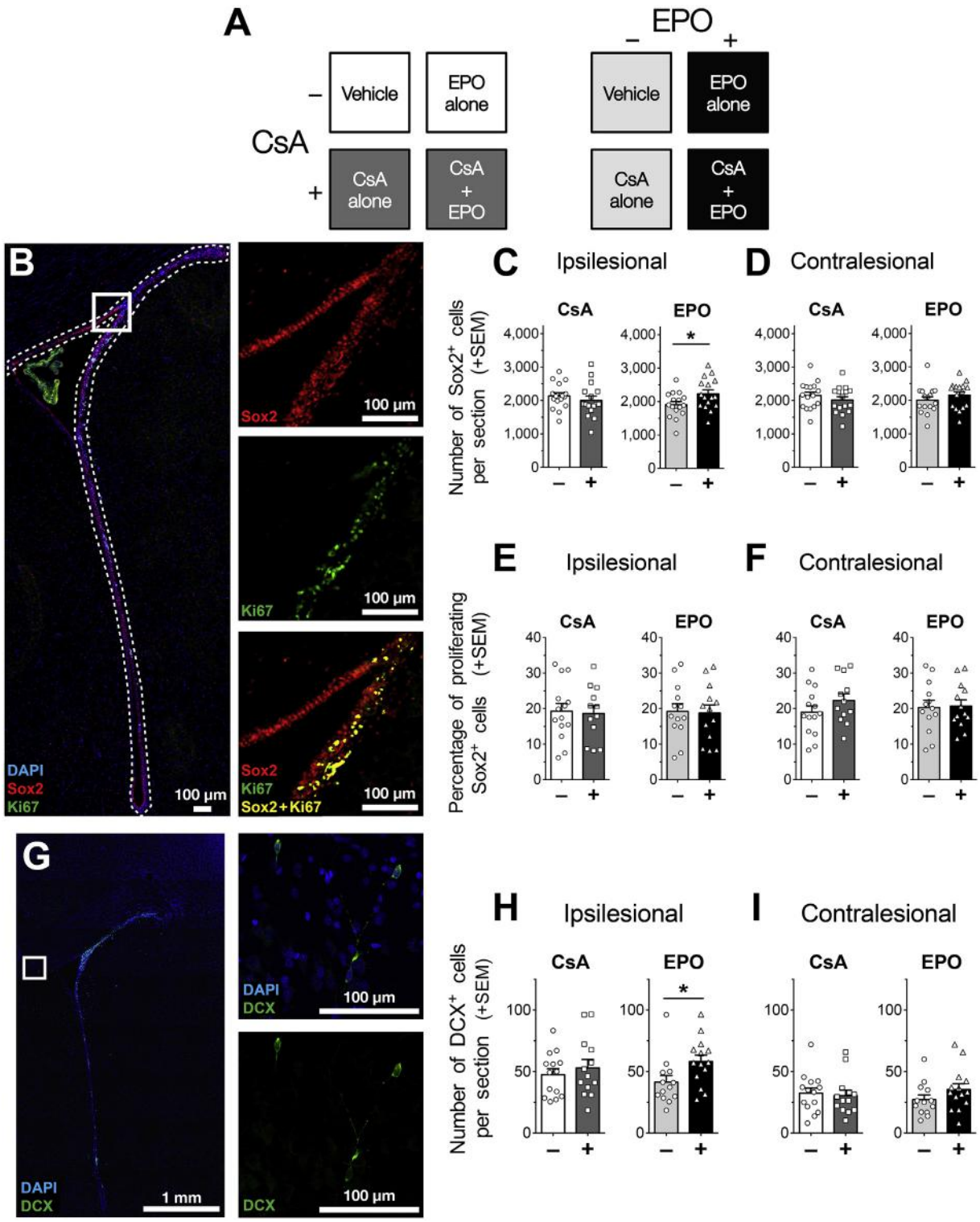

Fig. 4. EPO treatment increases the number of NSPCs and migrating neural progenitors. (A) Schematic of 2 × 2 factorial design used to assess individual drug effects. Groups were collapsed to compare CsA treatment (CsA-alone and CsA + EPO) to non-CsA treatment (vehicle and EPO-alone), and EPO treatment (EPO-alone and CsA + EPO) to non-EPO treatment (vehicle and CsA-alone). **(B)** Representative images of lateral ventricles (dashed outline) stained with Sox2 (red) for NSPCs and Ki67 (green) for proliferating cells. **(C, D)** Quantification of $Sox2^+$ cells in the (C) ipsilesional and (D) contralesional lateral ventricles, demonstrating increased number of NSPCs with EPO treatment (n = 16 rats per group). **(D, F)** Quantification of proliferating NSPCs, expressed as % of NSPCs that are proliferating in the (D) ipsilesional and (F) contralesional ventricles (non-CsA, n = 14 rats; CsA, n = 12; non-EPO, n = 13, EPO, n = 13). **(G)** Representative image of migrating DCX^+ neuroblasts (green) located outside the ventricles. **(H, I)** Quantification of DCX^+ neural progenitors located outside the ventricles in the (H) ipsilesional and (I) contralesional hemispheres, demonstrating increased number of migratory neuroblasts with EPO treatment (non-CsA, n = 14 rats; CsA, n = 13; non-EPO, n = 13, EPO, n = 14). Data are expressed as mean + s.e.m and all data points represent individual rats. Significance was evaluated by a two-way ANOVA (CsA x EPO) in each of C–F, H and I; *p < 0.05. (For interpretation of the references to colour in this figure legend, the reader is referred to the Web version of this article.)

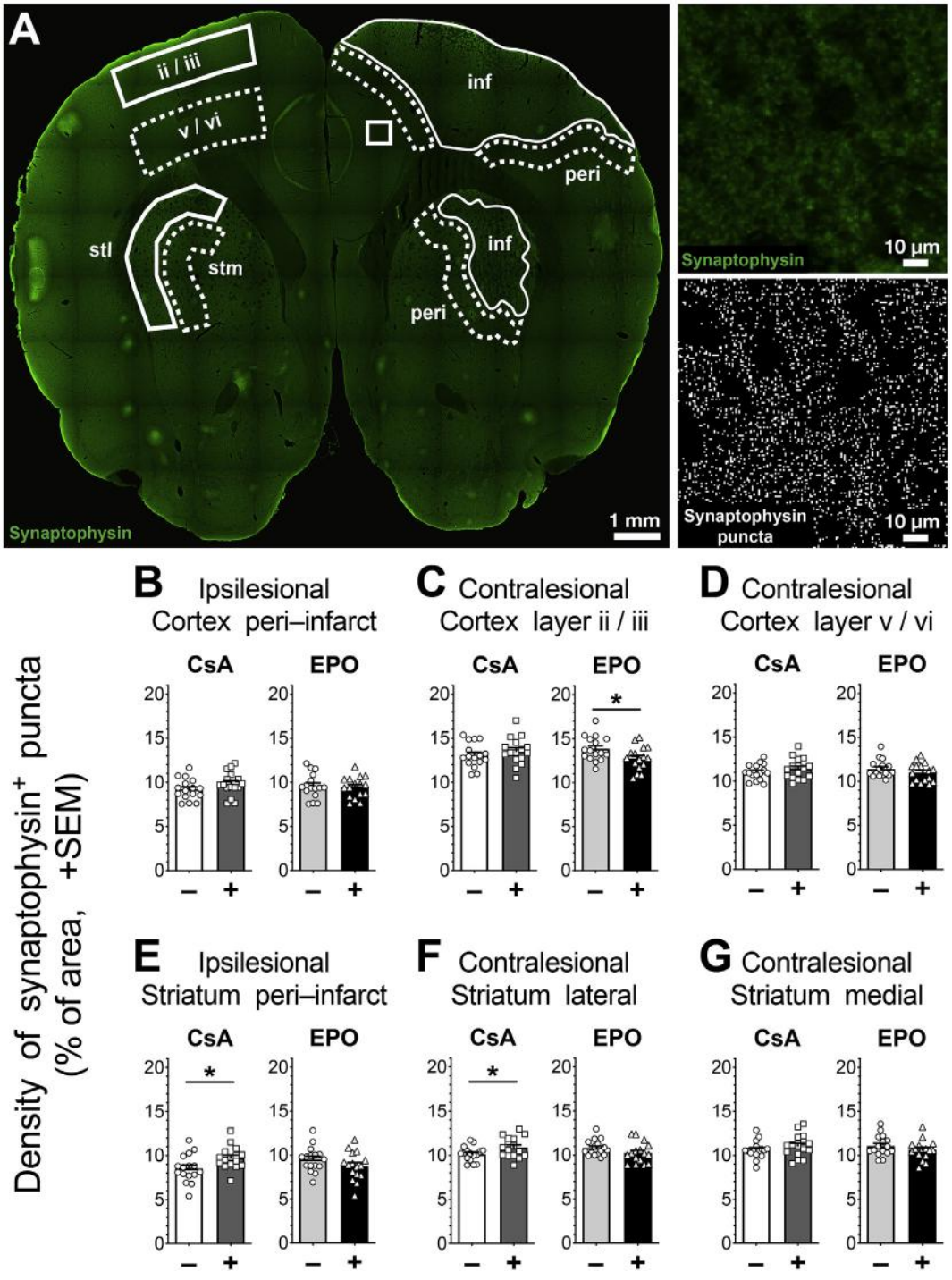

Fig. 5. Synaptic plasticity is differentially affected by CsA and EPO. (A) Representative image of synaptophysin staining and puncta in stroke-injured animals with quantification regions demarcated in the ipsilesional (inf = infarct; peri = peri-infarct) and contralesional (ii/iii = cortex layers ii and ii; v/vi = cortex layers v and vi; stl = striatum lateral; stm = striatum medial) hemispheres. **(B–D)** Quantification of synaptophysin puncta density, expressed as % synaptophysin$^+$ area, in the (B) ipsilesional cortical peri-infarct, (C) contralesional cortical layers ii/iii, and (D) contralesional cortical layers v/vi, demonstrating decreased plasticity with EPO-treated groups vs. EPO-untreated groups (n = 16 rats per group). (**E-G**) Quantification of synaptophysin puncta density in the (E) ipsilesional striatial peri-infarct, (F) contralesional lateral striatum, and (G) contralesional medial striatum, demonstrating increased plasticity with CsA-treated groups vs. CsA-untreated groups. Data are expressed as mean + s.e.m and all data points represent individual rats. Significance was evaluated by a two-way ANOVA (CsA x EPO) in each of B-G; *$p < 0.05$.

4. Discussion

The development of effective treatment strategies for neurological injuries, such as stroke, is becoming increasingly important as morbidity continues to rise. The lack of effective treatments remains an unmet challenge. Here we demonstrate novel drug combinations to be investigated, using a local delivery platform, which would otherwise be prohibited by traditional systemic strategies. While both CsA and EPO can cross the blood-brain barrier to a small extent, drug accumulation in the brain after systemic delivery to rats and humans is low

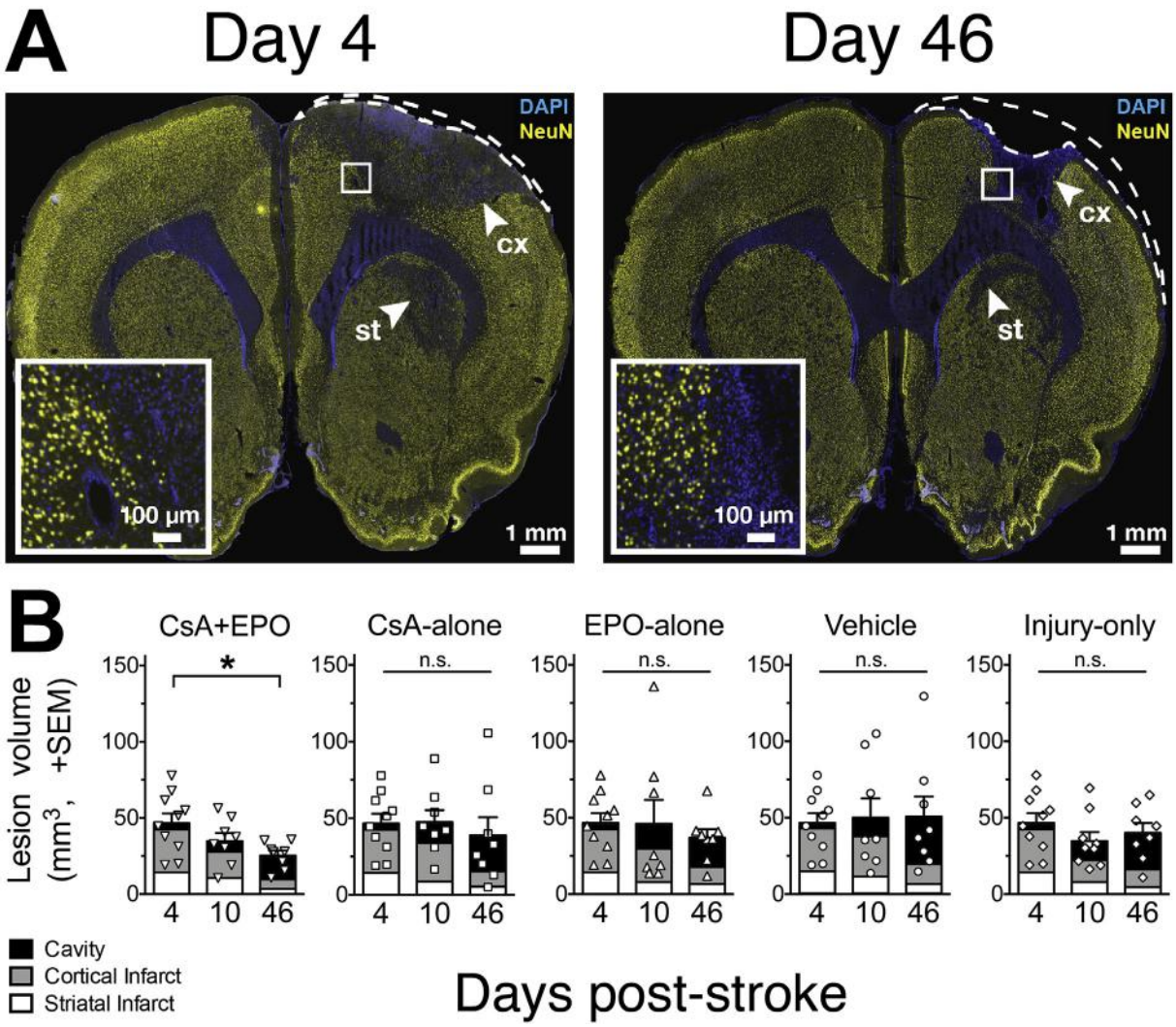

Fig. 6. Stroke lesion volume is decreased only by combined CsA and EPO delivery. (A) Representative images of stroke-injured brains stained with NeuN for mature neurons, demonstrating a change in injury composition over time. The cavity (dashed outline) is demarcated by the loss of DAPI staining and the infarct (arrowheads) in the cortex (cx) and striatum (st) is demarcated by the loss of NeuN staining relative to the uninjured contralesional hemisphere. (B) Quantification of lesion volume, defined as the sum of the cavity, cortical infarct and striatal infarct, before implant at day 4 (n = 10 rats) and after implant at day 10 (Injury-only, n = 9 rats; all other groups n = 8 rats) and day 46 (n = 8 rats per group) post-stroke, demonstrating decreased stroke lesion volume with CsA + EPO treatment. Data are expressed as mean + s.e.m and all data points represent individual rats. Significance was evaluated by a one-way ANOVA with Dunnett's post-hoc test vs. day 4 (2 comparisons); *$p < 0.05$.

($\sim 10^{-2}$ µg CsA/g tissue [6] and $\sim 10^{-1}$ ng EPO/g tissue [60]). Additionally, the side effects of systemic CsA and EPO delivery to stroke patients would be unsafe: CsA causes immunosuppression [40] in already susceptible stroke patients [41,42], and EPO increases red blood cell density [43], which increases the risk of secondary ischemic occlusion and injury [44]. The concentrations of CsA and EPO that we achieved in the brain by bypassing the BBB with our epi-cortical delivery strategy were approximately 3 orders of magnitude greater than systemic delivery ($\sim 10^{1}$ µg CsA/g tissue and $\sim 10^{2}$ ng EPO/g tissue). The benefit of localized drug delivery to the brain was demonstrated: high local concentrations were achieved using substantially less drug than required for systemic delivery [34,61] and there were very low drug concentrations in systemic organs [6].

We showed that functional recovery after stroke is possible using a local drug delivery paradigm where two drugs, CsA and EPO, were released directly to brain tissue. CsA + EPO treatment resulted in accelerated recovery of gross and fine motor functions compared to single-drug and vehicle treatments, with improvements observed as early as 10 days post-stroke. We attributed the accelerated recovery to our local drug delivery system, which provided high concentrations in the brain during the first weeks after injection. Other animal groups spontaneously improved to some degree at the later time points and no significant differences between groups were found at days 32 and 46, reflecting a limitation of the focal ischemia animal model. The Et-1 model mimics the size and injury evolution of treatable human stroke; however, more spontaneous recovery can occur in this model than is typically observed in the middle cerebral artery occlusion model, which produces very large injuries that mimic fatal human stroke [47,62]. The accelerated recovery with CsA + EPO in a model of treatable human stroke was significant and may have even greater benefit when combined with rehabilitation therapy, which is most effective within the first few weeks after human stroke [63].

Unlike neuroprotective therapies, which may be effective in the first few hours after injury [30], we showed that the CsA + EPO treatment is effective in treating sub-acute stroke, when administered 4 days after injury. This combination has never been studied in a sub-acute injury model. Only one previous study investigated systemic delivery of CsA + EPO in an acute stroke model; however, delivery begun within 30 min of ischemia and only tissue-level effects were reported. No additional functional recovery was observed with the combination

therapy in that study [38].

We investigated tissue repair in order to understand the mechanism for functional recovery. The fact that the treatment was applied 4 days after stroke, past the window for neuroprotection [39], suggests mechanisms of neurogenesis and plasticity [64]. Only EPO treatment (EPO alone or CsA + EPO) increased the number of NSPCs in the stroke-injured brain; yet, in the absence of any effect on NSPC proliferation, EPO likely impacted NSPC survival, which is consistent with previous reports [36,37,65]. With EPO treatment there was also a decrease in plasticity in layers ii/iii of the contralesional cortical hemisphere, which contain cross-hemispheric projections. Inhibiting contralesional sprouting has been demonstrated to improve outcomes after stroke [66] as sprouting of contralesional axons in layers ii/iii after stroke may be maladaptive [67]. Thus, EPO may have reduced maladaptive plasticity in the contralesional cortex. Yet, while EPO stimulated endogenous NSPCs and inhibited contralesional plasticity independent of CsA, this was insufficient for recovery of fine or gross motor skills. In the striatum, which is critical in forelimb reaching tasks [68], CsA treatment (CsA alone or CsA + EPO) increased plasticity in both the ipsilesional peri-infarct and the contralesional lateral striatum (Fig. 5C) whereas EPO had no effect. There is no known direct mechanism for CsA to increase synaptogenesis, but CsA has been shown to increase brain-derived neurotrophic factor expression in ischemic astrocytes, which in turn affects plasticity [69]. This mechanism may have played a role in our system as well; however, CsA alone was insufficient for functional recovery. We attribute the different effects of CsA and EPO to the overall tissue and functional benefit observed by their combined delivery. It was only in the combination group that we observed greater numbers of endogenous NSPCs, inhibition of contralesional plasticity, and increased striatal plasticity, demonstrating the necessity of stimulating multiple reparative mechanisms for functional recovery.

To advance towards the clinic, this strategy can be tested in alternative stroke models, like the middle cerebral artery occlusion, and in larger animals. Furthermore, the platform can be tested in other injury models where the mechanisms of neurogenesis and plasticity are also important to recovery, such as traumatic brain injury. Although drug diffusion was adequate to target the rat brain, and likely sufficient to target cortical tissue in the human brain [70], modifications to this strategy may be necessary to target deeper brain structures in larger brains. To increase their tissue penetration, drugs have been modified with poly(ethylene glycol), which decreases elimination from the tissue, effectively increasing diffusivity [11].

By demonstrating the feasibility of this platform strategy in a rat model of stroke, we open up the methodology for the delivery of a broader range of drug therapies in the treatment of different disorders or diseases, such as delivering glial-derived neurotrophic factor, a drug that cannot cross the BBB, to treat Parkinson's disease [71]. As our platform system is modular, single- or multi-drug release with independently tunable release rates is easily achievable. In the case of therapeutics that are unstable and cannot be delivered systemically, such as the glial-scar degrading enzyme chondroitinase ABC, an effective local delivery strategy is integral to success [16,29,72,73].

The approach is also compatible with other treatment modalities. As we show that our platform strategy itself does not affect behavioral performance in un-injured (or injured) animals, it can be combined with rehabilitation therapy, which may improve chronic outcomes. Importantly, with our local delivery system, drugs that were previously discarded for reasons of safety or their inability to cross the blood brain barrier can now be tested for tissue and functional repair in stroke and other neurological injuries and/or diseases.

Author contributions

A.T. designed the experiments, performed data analysis and wrote the manuscript. A.T., J.M.O, S.L.P. and R.C.W.S. carried out experiments. S.Z. assisted with experiments. C.M.M. designed the experiments and edited the manuscript. M.S.S. supervised the project, designed the experiments and edited the manuscript. All authors revised the manuscript.

Data availability

The processed data required to reproduce these findings are available to download from https://doi:10.17632/g3frn334tx.4 [74].

Declaration of competing interest

The authors declare no competing financial interests, but MSS acknowledges a composition of matter patent on HAMC.

Acknowledgments

We thank members of the Shoichet lab for thoughtful review of this manuscript. We are grateful to the Canadian Institutes of Health Research (CIHR, Foundation grant to MSS and project grant to CMM), the Ontario Graduate Scholarship (AT, JMO, SLP), and the Natural Sciences and Engineering Research Council (NSERC, CGS-D to JMO and SLP, and CREATE M3 to AT) for funding this research.

Appendix A. Supplementary data

Supplementary data to this article can be found online at https://doi.org/10.1016/j.biomaterials.2020.119794.

References

[1] E.J. Benjamin, S.S. Virani, C.W. Callaway, A.M. Chamberlain, A.R. Chang, S. Cheng, et al., Heart disease and stroke statistics-2018 update: a report from the American heart association, Circulation 137 (2018) e67–e492, https://doi.org/10.1161/CIR.0000000000000558.

[2] P.S. Briquez, L.E. Clegg, M.M. Martino, F.M. Gabhann, J.A. Hubbell, Design principles for therapeutic angiogenic materials, Nat. Rev. Mater. 1 (2016) 15006, https://doi.org/10.1038/natrevmats.2015.6.

[3] S.I. Rapoport, Osmotic opening of the blood-brain barrier: principles, mechanism, and therapeutic applications, Cell. Mol. Neurobiol. 20 (2000) 217–230.

[4] S. Joshi, A. Ergin, M. Wang, R. Reif, J. Zhang, J.N. Bruce, et al., Inconsistent blood brain barrier disruption by intraarterial mannitol in rabbits: implications for chemotherapy, J. Neuro Oncol. 104 (2011) 11–19, https://doi.org/10.1007/s11060-010-0466-4.

[5] K. Hynynen, N. McDannold, N.A. Sheikov, F.A. Jolesz, N. Vykhodtseva, Local and reversible blood-brain barrier disruption by noninvasive focused ultrasound at frequencies suitable for trans-skull sonications, Neuroimage 24 (2005) 12–20, https://doi.org/10.1016/j.neuroimage.2004.06.046.

[6] A. Tuladhar, C.M. Morshead, M.S. Shoichet, Circumventing the blood-brain barrier: local delivery of cyclosporin A stimulates stem cells in stroke-injured rat brain, J. Control. Release 215 (2015) 1–11, https://doi.org/10.1016/j.jconrel.2015.07.023.

[7] B. Kolb, C. Morshead, C. Gonzalez, M. Kim, C. Gregg, T. Shingo, et al., Growth factor-stimulated generation of new cortical tissue and functional recovery after stroke damage to the motor cortex of rats, J. Cereb. Blood Flow Metab. 27 (2007) 983–997, https://doi.org/10.1038/sj.jcbfm.9600402.

[8] W.M. Pardridge, Drug transport in brain via the cerebrospinal fluid, Fluids Barriers CNS 8 (2011) 7, https://doi.org/10.1186/2045-8118-8-7.

[9] P.A. Mead, J.E. Safdieh, P. Nizza, S. Tuma, K.A. Sepkowitz, Ommaya reservoir infections: a 16-year retrospective analysis, J. Infect. 68 (2014) 225–230, https://doi.org/10.1016/j.jinf.2013.11.014.

[10] M.J. Cooke, Y. Wang, C.M. Morshead, M.S. Shoichet, Controlled epi-cortical delivery of epidermal growth factor for the stimulation of endogenous neural stem cell proliferation in stroke-injured brain, Biomaterials 32 (2011) 5688–5697, https://doi.org/10.1016/j.biomaterials.2011.04.032.

[11] Y. Wang, M.J. Cooke, Y. Lapitsky, R.G. Wylie, N. Sachewsky, D. Corbett, et al., Transport of epidermal growth factor in the stroke-injured brain, J. Control. Release 149 (2011) 225–235, https://doi.org/10.1016/j.jconrel.2010.10.022.

[12] Y. Wang, M.J. Cooke, C.M. Morshead, M.S. Shoichet, Hydrogel delivery of erythropoietin to the brain for endogenous stem cell stimulation after stroke injury, Biomaterials 33 (2012) 2681–2692, https://doi.org/10.1016/j.biomaterials.2011.12.031.

[13] M.J. Caicco, M.J. Cooke, Y. Wang, A. Tuladhar, C.M. Morshead, M.S. Shoichet, A hydrogel composite system for sustained epi-cortical delivery of Cyclosporin A to the brain for treatment of stroke, J. Control. Release 166 (2013) 197–202, https://doi.org/10.1016/j.jconrel.2013.01.002.

[14] Y. Wang, M.J. Cooke, N. Sachewsky, C.M. Morshead, M.S. Shoichet, Bioengineered sequential growth factor delivery stimulates brain tissue regeneration after stroke,

J. Control. Release 172 (2013) 1–11, https://doi.org/10.1016/j.jconrel.2013.07.032.
[15] J.M. Obermeyer, A. Tuladhar, S.L. Payne, E. Ho, C.M. Morshead, M.S. Shoichet, Local delivery of brain-derived neurotrophic factor enables behavioral recovery and tissue repair in stroke-injured rats, Tissue Eng. A 25 (2019) 1175–1187, https://doi.org/10.1089/ten.TEA.2018.0215.
[16] M.H. Hettiaratchi, M.J. O'Meara, C.J. Teal, S.L. Payne, A.J. Pickering, M.S. Shoichet, Local delivery of stabilized chondroitinase ABC degrades chondroitin sulfate proteoglycans in stroke-injured rat brains, J. Control. Release 297 (2019) 14–25, https://doi.org/10.1016/j.jconrel.2019.01.033.
[17] D.F. Emerich, E. Silva, O. Ali, D. Mooney, W. Bell, S.-J. Yu, et al., Injectable VEGF hydrogels produce near complete neurological and anatomical protection following cerebral ischemia in rats, Cell Transplant. 19 (2010) 1063–1071, https://doi.org/10.3727/096368910X498278.
[18] H. Zhang, T. Hayashi, K. Tsuru, K. Deguchi, M. Nagahara, S. Hayakawa, et al., Vascular endothelial growth factor promotes brain tissue regeneration with a novel biomaterial polydimethylsiloxane-tetraethoxysilane, Brain Res. 1132 (2007) 29–35, https://doi.org/10.1016/j.brainres.2006.09.117.
[19] R. Ju, Y. Wen, R. Gou, Y. Wang, Q. Xu, The experimental therapy on brain ischemia by improvement of local angiogenesis with tissue engineering in the mouse, Cell Transplant. 23 (Suppl 1) (2014) S83–S95, https://doi.org/10.3727/096368914X684998.
[20] J. Ma, W.-M. Tian, S.-P. Hou, Q.Y. Xu, M. Spector, F.Z. Cui, An experimental test of stroke recovery by implanting a hyaluronic acid hydrogel carrying a Nogo receptor antibody in a rat model, Biomed. Mater. 2 (2007) 233–240, https://doi.org/10.1088/1748-6041/2/4/005.
[21] D.J. Cook, C. Nguyen, H.N. Chun, I.L. Llorente, A.S. Chiu, M. Machnicki, et al., Hydrogel-delivered brain-derived neurotrophic factor promotes tissue repair and recovery after stroke, J. Cereb. Blood Flow Metab. 37 (2017) 1030–1045, https://doi.org/10.1177/0271678X16649964.
[22] A.N. Clarkson, K. Parker, M. Nilsson, F.R. Walker, E.K. Gowing, Combined ampakine and BDNF treatments enhance poststroke functional recovery in aged mice via AKT-CREB signaling, J. Cereb. Blood Flow Metab. 35 (2015) 1272–1279, https://doi.org/10.1038/jcbfm.2015.33.
[23] K.J. Lampe, D.S. Kern, M.J. Mahoney, K.B. Bjugstad, The administration of BDNF and GDNF to the brain via PLGA microparticles patterned within a degradable PEG-based hydrogel: protein distribution and the glial response, J. Biomed. Mater. Res. 96 (2011) 595–607, https://doi.org/10.1002/jbm.a.33011.
[24] L. Mo, Z. Yang, A. Zhang, X. Li, The repair of the injured adult rat hippocampus with NT-3-chitosan carriers, Biomaterials 31 (2010) 2184–2192, https://doi.org/10.1016/j.biomaterials.2009.11.078.
[25] K. Nakaguchi, H. Jinnou, N. Kaneko, M. Sawada, T. Hikita, S. Saitoh, et al., Growth factors released from gelatin hydrogel microspheres increase new neurons in the adult mouse brain, Stem Cell. Int. 2012 (2012) 915160, , https://doi.org/10.1155/2012/915160.
[26] D. Gupta, C.H. Tator, M.S. Shoichet, Fast-gelling injectable blend of hyaluronan and methylcellulose for intrathecal, localized delivery to the injured spinal cord, Biomaterials 27 (2006) 2370–2379, https://doi.org/10.1016/j.biomaterials.2005.11.015.
[27] M.M. Pakulska, I. Elliott Donaghue, J.M. Obermeyer, A. Tuladhar, C.K. McLaughlin, T.N. Shendruk, et al., Encapsulation-free controlled release: electrostatic adsorption eliminates the need for protein encapsulation in PLGA nanoparticles, Sci. Adv. 2 (2016) e1600519, , https://doi.org/10.1126/sciadv.1600519.
[28] M.D. Baumann, C.E. Kang, J.C. Stanwick, Y. Wang, H. Kim, Y. Lapitsky, et al., An injectable drug delivery platform for sustained combination therapy, J. Control. Release 138 (2009) 205–213, https://doi.org/10.1016/j.jconrel.2009.05.009.
[29] M.M. Pakulska, C.H. Tator, M.S. Shoichet, Local delivery of chondroitinase ABC with or without stromal cell-derived factor 1α promotes functional repair in the injured rat spinal cord, Biomaterials 134 (2017) 13–21, https://doi.org/10.1016/j.biomaterials.2017.04.016.
[30] M.D. Ginsberg, Neuroprotection for ischemic stroke: past, present and future, Neuropharmacology 55 (2008) 363–389, https://doi.org/10.1016/j.neuropharm.2007.12.007.
[31] C. Wiltrout, B. Lang, Y. Yan, R.J. Dempsey, R. Vemuganti, Repairing brain after stroke: a review on post-ischemic neurogenesis, Neurochem. Int. 50 (2007) 1028–1041, https://doi.org/10.1016/j.neuint.2007.04.011.
[32] C.R. Stiller, J. Dupré, M. Gent, M.R. Jenner, P.A. Keown, A. Laupacis, et al., Effects of cyclosporine immunosuppression in insulin-dependent diabetes mellitus of recent onset, Science 223 (1984) 1362–1367.
[33] A. Erlandsson, C.-H.A. Lin, F. Yu, C.M. Morshead, Immunosuppression promotes endogenous neural stem and progenitor cell migration and tissue regeneration after ischemic injury, Exp. Neurol. 230 (2011) 48–57, https://doi.org/10.1016/j.expneurol.2010.05.018.
[34] N. Sachewsky, J. Hunt, M.J. Cooke, A. Azimi, T. Zarin, C. Miu, et al., Cyclosporin A enhances neural precursor cell survival in mice through a calcineurin-independent pathway, Dis. Model Mech. 7 (2014) 953–961, https://doi.org/10.1242/dmm.014480.
[35] C. Brugnara, L.A. Chambers, E. Malynn, M.A. Goldberg, M.S. Kruskall, Red blood cell regeneration induced by subcutaneous recombinant erythropoietin: iron-deficient erythropoiesis in iron-replete subjects, Blood 81 (1993) 956–964.
[36] L. Wang, Z. Zhang, Y. Wang, R. Zhang, M. Chopp, Treatment of stroke with erythropoietin enhances neurogenesis and angiogenesis and improves neurological function in rats, Stroke 35 (2004) 1732–1737, https://doi.org/10.1161/01.STR.0000132196.49028.a4.
[37] P.T. Tsai, J.J. Ohab, N. Kertesz, M. Groszer, C. Matter, J. Gao, et al., A critical role of erythropoietin receptor in neurogenesis and post-stroke recovery, J. Neurosci. 26 (2006) 1269–1274, https://doi.org/10.1523/JNEUROSCI.4480-05.2006.
[38] C.-M. Yuen, C.-K. Sun, Y.-C. Lin, L.-T. Chang, Y.-H. Kao, C.-H. Yen, et al., Combination of cyclosporine and erythropoietin improves brain infarct size and neurological function in rats after ischemic stroke, J. Transl. Med. 9 (2011) 141, https://doi.org/10.1186/1479-5876-9-141.
[39] M.D. Ginsberg, Current status of neuroprotection for cerebral ischemia: synoptic overview, Stroke 40 (2009), https://doi.org/10.1161/STROKEAHA.108.528877 S111–S114.
[40] R.M. Graham, Cyclosporine: mechanisms of action and toxicity, Clevel. Clin. J. Med. 61 (1994) 308–313.
[41] U. Dirnagl, J. Klehmet, J.S. Braun, H. Harms, C. Meisel, T. Ziemssen, et al., Stroke-Induced immunodepression: experimental evidence and clinical relevance, Stroke 38 (2007) 770–773, https://doi.org/10.1161/01.STR.0000251441.89665.bc.
[42] K. Shi, K. Wood, F.-D. Shi, X. Wang, Q. Liu, Stroke-induced immunosuppression and poststroke infection, Stroke Vasc Neurol 3 (2018) 34–41, https://doi.org/10.1136/svn-2017-000123.
[43] S.T. Provatopoulou, P.N. Ziroyiannis, Clinical use of erythropoietin in chronic kidney disease: outcomes and future prospects, Hippokratia 15 (2011) 109–115.
[44] C. Ani, B. Ovbiagele, Elevated red blood cell distribution width predicts mortality in persons with known stroke, J. Neurol. Sci. 277 (2009) 103–108, https://doi.org/10.1016/j.jns.2008.10.024.
[45] H.K. Makadia, S.J. Siegel, Poly lactic-co-glycolic acid (PLGA) as biodegradable controlled drug delivery carrier, Polymers 3 (2011) 1377–1397, https://doi.org/10.3390/polym3031377.
[46] B.S. Zolnik, D.J. Burgess, Effect of acidic pH on PLGA microsphere degradation and release, J. Control. Release 122 (2007) 338–344, https://doi.org/10.1016/j.jconrel.2007.05.034.
[47] S.T. Carmichael, Rodent models of focal stroke: size, mechanism, and purpose, NeuroRx 2 (2005) 396–409, https://doi.org/10.1602/neurorx.2.3.396.
[48] C. Nguemeni, M. Gomez-Smith, M.S. Jeffers, C.P. Schuch, D. Corbett, Time course of neuronal death following endothelin-1 induced focal ischemia in rats, J. Neurosci. Methods 242 (2015) 72–76, https://doi.org/10.1016/j.jneumeth.2015.01.005.
[49] M.C. Jimenez Hamann, E.C. Tsai, C.H. Tator, M.S. Shoichet, Novel intrathecal delivery system for treatment of spinal cord injury, Exp. Neurol. 182 (2003) 300–309.
[50] M. Fisher, G. Feuerstein, D.W. Howells, P.D. Hurn, T.A. Kent, S.I. Savitz, et al., Update of the stroke therapy academic industry roundtable preclinical recommendations, Stroke 40 (2009) 2244–2250, https://doi.org/10.1161/STROKEAHA.108.541128.
[51] V. Windle, A. Szymanska, S. Granter-Button, C. White, R. Buist, J. Peeling, et al., An analysis of four different methods of producing focal cerebral ischemia with endothelin-1 in the rat, Exp. Neurol. 201 (2006) 324–334, https://doi.org/10.1016/j.expneurol.2006.04.012.
[52] M.S. Jeffers, A. Hoyles, C. Morshead, D. Corbett, Epidermal growth factor and erythropoietin infusion accelerate functional recovery in combination with rehabilitation, Stroke 45 (2014) 1856–1858, https://doi.org/10.1161/STROKEAHA.114.005464.
[53] C.T. Noguchi, P. Asavaritikrai, R. Teng, Y. Jia, Role of erythropoietin in the brain, Crit. Rev. Oncol. Hematol. 64 (2007) 159–171, https://doi.org/10.1016/j.critrevonc.2007.03.001.
[54] K.L. Schaar, M.M. Brenneman, S.I. Savitz, Functional assessments in the rodent stroke model, Exp. Transl. Stroke Med. 2 (2010) 13, https://doi.org/10.1186/2040-7378-2-13.
[55] M.G. Balkaya, R.C. Trueman, J. Boltze, D. Corbett, J. Jolkkonen, Behavioral outcome measures to improve experimental stroke research, Behav. Brain Res. (2017), https://doi.org/10.1016/j.bbr.2017.07.039.
[56] J. Schindelin, I. Arganda-Carreras, E. Frise, V. Kaynig, M. Longair, T. Pietzsch, et al., Fiji: an open-source platform for biological-image analysis, Nat. Methods 9 (2012) 676–682, https://doi.org/10.1038/nmeth.2019.
[57] C.M. Morshead, B.A. Reynolds, C.G. Craig, M.W. McBurney, W.A. Staines, D. Morassutti, et al., Neural stem cells in the adult mammalian forebrain: a relatively quiescent subpopulation of subependymal cells, Neuron 13 (1994) 1071–1082, https://doi.org/10.1016/0896-6273(94)90046-9.
[58] C.B. Johansson, S. Momma, D.L. Clarke, M. Risling, U. Lendahl, J. Frisen, Identification of a neural stem cell in the adult mammalian central nervous system, Cell 96 (1999) 25–34, https://doi.org/10.1016/S0092-8674(00)80956-3.
[59] T. Wieloch, K. Nikolich, Mechanisms of neural plasticity following brain injury, Curr. Opin. Neurobiol. 16 (2006) 258–264, https://doi.org/10.1016/j.conb.2006.05.011.
[60] F. Zhang, J. Xing, A.K.-F. Liou, S. Wang, Y. Gan, Y. Luo, et al., Enhanced delivery of erythropoietin across the blood-brain barrier for neuroprotection against ischemic neuronal injury, Transl. Stroke Res. 1 (2010) 113–121, https://doi.org/10.1007/s12975-010-0019-3.
[61] L. Belayev, L. Khoutorova, K.L. Zhao, A.W. Davidoff, A.F. Moore, S.C. Cramer, A novel neurotrophic therapeutic strategy for experimental stroke, Brain Res. 1280 (2009) 117–123, https://doi.org/10.1016/j.brainres.2009.05.030.
[62] R.B. Roome, R.F. Bartlett, M. Jeffers, J. Xiong, D. Corbett, J.L. Vanderluit, A reproducible Endothelin-1 model of forelimb motor cortex stroke in the mouse, J. Neurosci. Methods 233 (2014) 34–44, https://doi.org/10.1016/j.jneumeth.2014.05.014.
[63] D. Corbett, M. Jeffers, C. Nguemeni, M. Gomez-Smith, J. Livingston-Thomas, Lost in Translation: Rethinking Approaches to Stroke Recovery, first ed., Elsevier B.V, 2015, https://doi.org/10.1016/bs.pbr.2014.12.002.
[64] S.T. Carmichael, The 3 Rs of stroke biology: radial, Relayed Regen. 13 (2016) 348–359, https://doi.org/10.1007/s13311-015-0408-0.
[65] T. Shingo, S.T. Sorokan, T. Shimazaki, S. Weiss, Erythropoietin regulates the in vitro and in vivo production of neuronal progenitors by mammalian forebrain neural

stem cells, J. Neurosci. 21 (2001) 9733–9743.
[66] B.K. Mansoori, L. Jean-Charles, B. Touvykine, A. Liu, S. Quessy, N. Dancause, Acute inactivation of the contralesional hemisphere for longer durations improves recovery after cortical injury, Exp. Neurol. 254 (2014) 18–28, https://doi.org/10.1016/j.expneurol.2014.01.010.
[67] B. Touvykine, B.K. Mansoori, L. Jean-Charles, J. Deffeyes, S. Quessy, N. Dancause, The Effect of Lesion Size on the Organization of the Ipsilesional and Contralesional Motor Cortex, Neurorehabil Neural Repair, 2015, https://doi.org/10.1177/1545968315585356.
[68] M. Pisa, Motor functions of the striatum in the rat: critical role of the lateral region in tongue and forelimb reaching, Neuroscience 24 (1988) 453–463, https://doi.org/10.1016/0306-4522(88)90341-7.
[69] B. Gabryel, J. Bernacki, Effect of FK506 and cyclosporine A on the expression of BDNF, tyrosine kinase B and p75 neurotrophin receptors in astrocytes exposed to simulated ischemia in vitro, Cell Biol. Int. 33 (2009) 739–748, https://doi.org/10.1016/j.cellbi.2009.04.006.
[70] B. Fischl, A.M. Dale, Measuring the thickness of the human cerebral cortex from magnetic resonance images, Proc. Natl. Acad. Sci. U.S.A. 97 (2000) 11050–11055, https://doi.org/10.1073/pnas.200033797.
[71] X. d'Anglemont de Tassigny, A. Pascual, J. López-Barneo, GDNF-based therapies, GDNF-producing interneurons, and trophic support of the dopaminergic nigrostriatal pathway. Implications for Parkinson's disease, Front. Neuroanat. 9 (2015) 10, https://doi.org/10.3389/fnana.2015.00010.
[72] S. Soleman, P.K. Yip, D.A. Duricki, L.D.F. Moon, Delayed treatment with chondroitinase ABC promotes sensorimotor recovery and plasticity after stroke in aged rats, Brain 135 (2012) 1210–1223, https://doi.org/10.1093/brain/aws027.
[73] M.M. Pakulska, K. Vulic, M.S. Shoichet, Affinity-based release of chondroitinase ABC from a modified methylcellulose hydrogel, J. Control. Release 171 (2013) 11–16, https://doi.org/10.1016/j.jconrel.2013.06.029.
[74] A. Tuladhar, M.S. Shoichet, In vivo drug release, functional recovery and tissue repair in stroke-injured rats after local delivery of cyclosporine and erythropoietin from epi-cortically implanted hyaluronan and methylcellulose (HAMC) hydrogel, Mendeley Data V4 (2020), https://doi.org/10.17632/g3frn334tx.4.